



**UNIVERSITY OF LEEDS**

This is a repository copy of *Experimental photothermal performance of nanofluids under concentrated solar flux*.

White Rose Research Online URL for this paper:  
<http://eprints.whiterose.ac.uk/133624/>

Version: Accepted Version

---

**Article:**

Amjad, M, Jin, H, Du, X et al. (1 more author) (2018) Experimental photothermal performance of nanofluids under concentrated solar flux. *Solar Energy Materials and Solar Cells*, 182. pp. 255-262. ISSN 0927-0248

<https://doi.org/10.1016/j.solmat.2018.03.044>

---

© 2018 Elsevier B.V. This manuscript version is made available under the CC-BY-NC-ND 4.0 license <http://creativecommons.org/licenses/by-nc-nd/4.0/>.

**Reuse**

This article is distributed under the terms of the Creative Commons Attribution-NonCommercial-NoDerivs (CC BY-NC-ND) licence. This licence only allows you to download this work and share it with others as long as you credit the authors, but you can't change the article in any way or use it commercially. More information and the full terms of the licence here: <https://creativecommons.org/licenses/>

**Takedown**

If you consider content in White Rose Research Online to be in breach of UK law, please notify us by emailing [eprints@whiterose.ac.uk](mailto:eprints@whiterose.ac.uk) including the URL of the record and the reason for the withdrawal request.



[eprints@whiterose.ac.uk](mailto:eprints@whiterose.ac.uk)  
<https://eprints.whiterose.ac.uk/>

# Experimental assessment of the photothermal conversion performance of six nanofluids

Muhammad Amjad<sup>1,2</sup>, Ghulam Raza<sup>1</sup>, Haichuan Jin<sup>1,4</sup>, Xiaoze Du<sup>3</sup>, Dongsheng Wen<sup>1,4\*</sup>

<sup>1</sup> School of Chemical and Process Engineering, University of Leeds, Leeds, LS2 9JT, UK

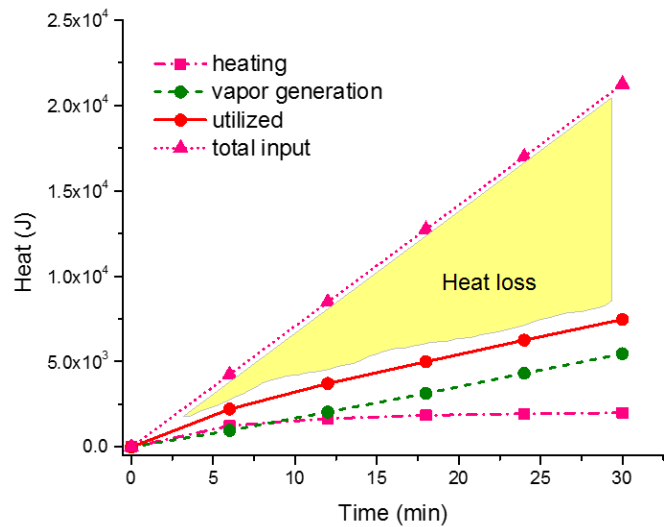
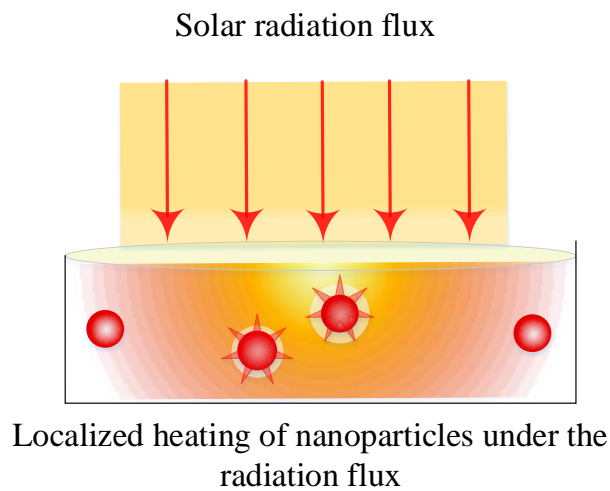
<sup>2</sup> Department of Mechanical Engineering, University of Engineering and Technology Lahore (KSK Campus), Pakistan.

<sup>3</sup> School of Energy, Power and Mechanical Engineering, North China Electric University, Beijing 102206, P.R.China.

<sup>4</sup> School of Aeronautic Science and Engineering, Beihang University, Beijing, 100191, P.R.China

**Abstract:** Nanoparticle-based direct solar absorption is a promising technology for future solar thermal systems. Having so many individual studies on different nanomaterials independently for solar energy harness, a comprehensive comparison of photothermal conversion characteristics of various nanofluids at the same experimental conditions is much needed. The photothermal conversion performance of six commonly used nanomaterials in direct absorption solar collectors (DASC) is investigated under a focused solar simulator (i.e. 12 Suns) with deionized water as the base fluid. The concentration of each nanofluid is kept the same, and their photothermal efficiencies and specific absorption rates are determined. The results show that all the nanofluids have higher solar energy absorption than the base fluid and silver turned out to be the best amongst all. The photothermal conversion efficiency of silver is 52.2% and its enhancement in the photothermal performance is almost 100% over the base fluid within the experimental domain. In addition, the contribution of sensible heating and latent heat of vaporization to the photothermal performance of the nanofluids is revealed.

### Graphical abstract:



### Research Highlights:

- Photothermal performance of six mostly used nanofluids in direct absorption solar collection was studied quantitatively under similar experimental conditions.
- Silver and iron nanofluids enhanced photothermal conversion performance by 100% and 70.3% respectively as compared to deionized water
- Specific absorption rate of silver nanoparticle was 2.33 kW/g, which was the highest amongst all the nanofluids compared in this investigation.
- The enhancement in photothermal performance is examined quantitatively in terms of sensible heating and steam generation.

**Keywords:** Nanofluid, photothermal conversion, nanoparticle, direct absorption, sensible heat, vapor generation

## 1. Introduction

With increasing concerns over global warming and environmental issues, developing renewable energy is becoming more and more important to secure our energy needs. Solar energy is the most abundant source of energy and is easily accessible. However making efficient use of solar energy is not an easy task [1]. A conventional plate-type of solar collector absorbs solar energy on an absorbing plate, and transfers the heat via a wall to a working fluid running inside [2-4]. It is a surface-based absorption, which limits the effective utilization of solar energy by creating a large temperature difference between the absorbing plate and the working fluid, especially for concentrated solar energy applications [5].

The limitations of surface absorption can be mitigated by a volume based solar absorption in which the working fluid directly absorbs energy from the Sun, named as direct absorption solar collection (DASC). The concept has its origin back in 1970 [6] and is receiving an increasing interest and attention recently by using different nanoparticles [7-9]. Several nanomaterials like silver [7, 10], gold [11-13], carbon nanotubes [14-16], copper [17], aluminum oxide ( $\text{Al}_2\text{O}_3$ ) [1, 18-21], graphite [22], graphene [5], and titanium dioxide ( $\text{TiO}_2$ ) [2] have been examined experimentally as well as numerically [23-28] for their capabilities to enhance solar absorption individually. Light to thermal conversion characteristics of these nanofluids have been investigated at various concentrations. For example Enio et al. [10] examined Ag nanofluid in a volume concentration range of 0.0001625% to 0.065% while Zhang et al. [13] explored the effect of adding Au nanoparticles in DI water in the range of 0.00028% to 0.0112 wt%. Yousefi et al. [16] used 0.2 wt.% in water with varying pH values in a flat plate solar collector and

Qenbo et al. [17] employed Cu nanoparticles with 0.001% to 0.02% volume concentration. Similarly Yousefi et al. [21] used 0.2% and 0.4 wt% , Hament et al. [1] used 0.001% to 0.05% by volume and Said et al. [20] used 0.05% to 0.1% volume concentration of Al<sub>2</sub>O<sub>3</sub> nanoparticles. Except that Zhang et al. [29] who examined various types of nanoparticles at the same concentration under 1 Sun, each of the above mentioned study was based on only one particular type of particle. A comparative assessment of the performance of commonly used nanomaterials for solar energy harness is much needed. The effect of these nanomaterials must be investigated at the same concentration under similar operating conditions to reveal their photothermal conversion performance.

This study identified six most commonly used nanomaterials in direct absorption solar collectors and investigated their photothermal performance under a focused solar simulator (i.e., 12 Suns). The bulk temperature rise of the nanofluids was measured with the help of three K-type thermocouples under the LabVIEW environment. Their photothermal conversion efficiencies and specific rate of absorption were obtained for comparison and possible mechanisms were examined.

## **2. Materials and methods**

### **2.1. Materials**

Commercial nanopowders of six materials including Ag, Cu and Zn (Sigma Aldrich Co.) and Fe, Si and Al<sub>2</sub>O<sub>3</sub>- $\gamma$  (Nanostructured & amorphous material Inc.) were used as received. Tri-sodium citrate (99.8%, Fisher Scientific) was used as the dispersant and stabilizing agent and DI water was used as the base fluid throughout the experimental procedure.

## 2.2. Nanofluids preparation and their characterization

Different metallic nanopowders of Ag, Zn, Fe, Cu, Si and  $\text{Al}_2\text{O}_3\text{-}\gamma$  were selected to prepare nanofluids by the two-step method. In this method, selected nanopowders were directly mixed with a 0.5% of tri-sodium citrate solution in DI water. For instance, to prepare a nanofluid of 0.01% weight concentration, 0.01 g nanopowder was mixed with 99.99 g of a 0.5% aqueous solution of trisodium citrate (TSC) under vigorous stirring. The acquired mixture was sonicated by a high energy probe (1200 W) for 5 minutes where the temperature was controlled at 40°C. The suspensions were then cooled down naturally to the room temperature and were sonicated for 10 min before the photothermal conversion experiment.

Morphological characterization of the nanopowders is given in **Fig.1** where **Fig (I)** (a through f) shows scanning electron microscopic (SEM) images of the nanopowders and transmission electron microscopy (TEM) micrograph of silver nanopowder dispersed in 0.5% aqueous solution of TSC is given in **Fig.1 (II)**. The nanopowders were mostly clustered (**Fig.1 (I)**) before the dispersion but became completely dispersed in DI water in the presence of stabilizing agent after sonication. The dispersion stability can also be seen from the stable absorption spectra in **Fig.3**. The optical absorption of these nanofluids was checked by a UV-Visual spectrometer (UV-1800, Shimadzu) using a high precision cell (made of HOQ 310H) with light path of 10 mm. The primary particle size range of the nanopowders as supplied by the suppliers is given in **Table 1**.

## 2.3. Experimental setup

The photothermal conversion characteristics of the prepared nanofluids were investigated using a solar simulator (Newport Co.). It has a class AAA certification to JIS C 8912, and ASTM E 927-05 standards, which has a 450W xenon lamp as the light source and spectral correction

filters (known as Air Mass filters) to correct the light output to closely match the solar spectrum. An air mass filter AM1.5G was used to simulate the direct solar spectrum when the Sun was at a zenith angle of 48.20 (ASTM E891). The sun simulator has a spectral match 0.75-1.25% fraction of ideal percentage, 2% non-uniformity of irradiance and  $\pm 2\%$  spectral instability according to ASTM Class AAA standard. A schematic view of the experimental setup is presented in **Fig.2**.

A petri dish of 5.8 cm diameter was used to contain the sample. The bulk temperature change was measured by three K-type (Omega 5TC-TT-K-36-36) thermocouples (TC), which were positioned at an angular position of  $120^\circ$  at three representatively depths: just under the top surface of the fluid, at the middle and close to the bottom of the petri dish but not in contact. A fourth thermocouple was used to measure the variation of room temperature. The data were registered by a data acquisition device (NI SCXI-1303) under the LabVIEW environment at a sampling rate of 1 Hz. The uncertainty in temperature measurement was calibrated as  $\pm 0.25^\circ\text{C}$ . The sample container was rinsed with DI water before each experiment to avoid inter-sample contamination.

A Fresnel lens of  $5.5 \times 5.5 \text{ inch}^2$  with a focal length of 10 inch was used to focus the output light onto a nanofluid sample. The focused intensity of light was measured as 12 suns with the help of a solar intensity meter.

### **3. Results and analysis**

#### **3.1. Optical absorbance**

Water is a poor absorber of the solar energy in the visible light spectrum where most of the solar energy is contained as can be seen from **Fig. 3**. Solar absorption of water can be significantly enhanced by adding nanoparticles that have good absorptivity in the visible region. In this study,

the optical absorptivity of the prepared nanofluids was checked by a UV-Vis spectrometer using a high precision quartz cell with light path of 10 mm. The optical absorbance spectra and spectral solar irradiance are shown in **Fig. 3**.

Different metallic nanofluids have different optical absorption peaks over the visible spectrum. The absorption peak of silver nanoparticles is the strongest amongst all the nanofluids compared at the same particle concentration of 0.01 wt. % (**Fig. 3**). This is due to the strong localized surface plasmonic effect in silver nanoparticle that makes it different from the others. The plasmonic resonance frequency of silver nanofluid can be seen around 430 nm from **Fig. 3**, which is almost the beginning of the visible band of the solar spectrum.

Compared with silver, the optical absorbance of other nanofluids in this study has mostly their absorption peaks in the UV to visible region. Though the absorption peaks of Fe, Si, Cu nanofluids are not very strong in the UV region, the flat absorption curve in the visible region shows that their absorption is far much better than water at such a low weight concentration. The optical absorbance curve of  $\text{Al}_2\text{O}_3\text{-}\gamma$  nanofluid is almost similar to that of DI water in the visible region, which is also reflected in the temperature curves, as described below.

### **3.2. Bulk fluid temperature**

The temperature of the nanoparticles in the nanofluid can be assumed as the temperature of the bulk fluid due to very small nanoparticle concentration i.e. only 0.01% by weight. Deionized water and sample of each fluid was heated for a minimum period of 30 min under the solar flux of 12 suns. The bulk fluid temperature change was measured using three thermocouples and the average bulk temperature ( $\Delta T = (T_1 + T_2 + T_3)/3$ , where  $T_1$ ,  $T_2$  and  $T_3$  are temperatures measured by thermocouples TC1, TC2 and TC3 respectively) variation for different nanofluids is

given in **Fig.4**. The corresponding mass loss due to vaporization of the fluid was measured with a digital microbalance and is given in **Fig.5**.

As it can be clearly seen from **Fig.4** that the average temperature variation in all the fluid samples is almost linear at the start of the experiment, and this linearity is lost as the experiment is continued. Such a linearity at the start of the experiment is because almost all of the energy is absorbed by the nanofluid volume and there is negligible heat leakage to the surroundings, **Fig 6 (a)**. But as the temperature of the nanofluid increases, the temperature difference between the sample and the surrounding increases, which results in increased heat loss to the ambient and subsequently deviation from the linearity. As the temperature difference goes to the maximum value within the experimental settings, further rate of increase in temperature gets smaller and smaller, as can be seen at the later stage of the experiment in **Fig.4**. In comparison with deionized water, all of the nanofluids have higher temperature gradients. In the order of the nanofluids with respect to their peak temperature, silver nanofluid is at the highest position, followed by Fe, Zn, Cu and Si as can be seen from **Fig.4**.

### **3.3. Mass loss of nanofluids due to evaporation**

The mass loss of the sample due to vaporization was measured by an electronic scale, as shown in **Fig.2**, and is given in **Fig. 5** over a 30 min time period. The mass loss of the sample of DI water and nanofluid is proportional to the fluid bulk temperature rise shown in **Fig. 4**. Under the effect of a low light flux from the solar simulator, most of the energy was consumed in heating the bulk fluid at the initial stage of the experiment, as can be seen by the contribution of sensible heat and latent heat in **Fig. 6 (b)** for the case of silver nanofluid. But as the experiment proceeds, more absorbed energy is used to evaporate the fluid, instead of heating the bulk fluid. The heat

loss to the ambient increases with the increase in overall temperature of the sample volume (**Fig. 6 (b)**).

### 3.4. Photothermal efficiency

As the overall temperature of the nanofluid sample is small, it can be believed that temperature of the nanoparticles and the surrounding fluid is same. For smaller fluid depths and overall homogeneous temperature distribution in a fluid volume, the light to heat conversion transient efficiency  $\eta_{PTE}$  can be calculated by the relation in **Eq. (1)**;

$$\eta_{PTE} = \frac{\int_0^t (c_w m_w + c_n m_n) \cdot \Delta T \cdot dt + \int_0^t L_v \cdot m_{loss} \cdot dt}{\int_0^t I \cdot A_i \cdot dt} \quad (1)$$

where  $c$  and  $m$  represent the specific heat capacity (J/kgK) and mass (kg) and the subscripts  $w$  and  $n$  represent water and nanofluid respectively,  $\Delta T$  is the average ( $\Delta T = (T_1 + T_2 + T_3)/3$ ) change in temperature in time  $t$  of three thermocouples,  $I$  is the solar irradiance, which is equal to 11.6 kW/m<sup>2</sup> in this work and  $A_i$  is the illumination area of the nanofluid sample,  $L_v$  is the latent heat of vaporization of water at 1atm and  $m_{loss}$  is mass loss of the sample in time  $t$ . As the overall particle concentration is very small so the  $c_n m_n / c_w m_w \approx 0$ , and the **Eq. (1)** can be reduced to **Eq. (2)**;

$$\eta_{PTE} = \frac{\int_0^t c_w m_w \cdot \Delta T \cdot dt + \int_0^t L_v \cdot m_{loss} \cdot dt}{\int_0^t I \cdot A_i \cdot dt} \quad (2)$$

Light to heat conversion efficiency including sensible heating and vapor generation efficiencies of various nanosuspensions with 0.01 wt. % concentration for initial stage of heating for 6 min is shown in **Fig. 7 (a)** and for total experiment duration in **Fig 7. (b)**. Comparing with the base fluid, the photothermal conversion efficiencies of nanofluids are significantly high. The average fluid temperature from three thermocouples was used. Amongst all the nanofluids used in this study,

Ag has the highest efficiency as compared to the base fluid. The enhancement in efficiency over the experimental domain is shown in **Fig.8** while the inset shows the efficiency enhancement in the first 6 min duration over the base fluid.

### 3.5. Specific absorption rate

Other than photothermal efficiency, specific absorption rate (SAR) is an important quantitative tool to evaluate the ability of the nanoparticles to absorb energy absorption. The energy absorbed per unit mass of the nanoparticles is known as SAR, used to describe the photothermal performance of nanofluids. SAR (kW/g) of nanofluids can be calculated using **Eq. (3)**

$$SAR = \frac{[(c_w m_w + c_n m_n) \Delta T_n - c_w m_w \Delta T_w] + L_v \cdot m_{loss}}{1000 m_n \Delta t} \quad (3)$$

where  $c_w$  and  $m_w$  represent the specific heat capacity (J/kgK) and mass (kg) of base fluid and  $c_n$  and  $m_n$  represent specific heat capacity and mass of nanoparticles.  $\Delta T_n$  and  $\Delta T_w$  show the change in temperature of nanofluid and water in time  $\Delta t$  respectively. Within the scope of this work ( $(c_n \Delta T_n / (1000 \cdot \Delta t)) \sim 0$ ) and hence the SAR can be approximated as in **Eq. (4)**

$$SAR \approx \frac{c_w m_w (\Delta T_n - \Delta T_w) + L_v m_{loss}}{1000 \cdot m_n \Delta t} \quad (4)$$

**Fig. 9** shows the SAR of the nanofluids compared with the base fluid for a 0.01% concentration by weight. Clearly from **Fig. 9**, the SAR of silver nanoparticles is higher than any other nanoparticles and the results are consistent to that of Enio et al. [10]. The ability of plasmonic nanoparticles to absorb solar energy is much better than that of many magnetic nanoparticles under such a low light heat flux as described by [30]

## 4. Discussion

Photothermal performance of the nanoparticles suspended in a base fluid cannot be predicted reliably relying on their optical properties only as reported in numerous studies [25, 31-33]. The

photothermal conversion performance of different nanofluids is investigated experimentally based on transient bulk temperature rise and the latent heat of vaporization of the nanofluid sample in this study. All nanomaterials showed a significantly higher photo energy absorption behavior compared to the base fluid and the plasmonic silver nanofluid had the best performance, which is in accordance with various individual studies [7, 10].

The average bulk fluid temperature of three thermocouples and corresponding mass change due to vaporization were used to determine the photothermal conversion efficiency and specific absorption rate of the nanofluid samples to compare with the base fluid. The temperature variation is almost linear with time at the initial phase of exposure to solar flux and as the time elapse, this temperature gradient becomes flat (Fig. 4). The linear change in temperature at the start is due to the minimum heat loss to the ambient. At the later stage, the thermal loss to the surroundings suppresses the heat utilization, the overall photothermal efficiency of the system is decreased consequently.

The heat utilization and its distribution to sensible heat, latent heat and ambient loss for the case of silver nanofluid is shown in Fig. 6. The sensible heat and latent heat of vaporization of the silver nanosuspension as shown in Fig 6 (a) are almost equal at the very beginning of the experiment while the latent heat of vaporization part of the utilized energy keeps on increasing over the sensible heat part with the passage of time. This increasing trend of latent heat continues until the end of the experiment while the increase rate of sensible heat of the sample is very low especially at the last phase of the experiment. The corresponding efficiency of the sensible heating and vapor generation are shown Fig 6 (b), which shows a gradual decrease in overall photothermal performance of the silver suspension over the time. After 6 min of the experiment,

the efficiency of the sensible heating and that of vapor generation are 29.4% and 22.8% respectively, which are decreased to 9.4% and 25.7% after 30 min. A dramatic change in the heating efficiency over time shows a rapid loss of heat to the ambient while a slight variation in the vapor generation efficiency signifies that the strong localized heat by silver nanoparticles sustained vapor generation irrespective of the bulk fluid temperature within the experimental domain.

A comparison of heating efficiency and vapor generation efficiency of various nanofluids investigated based on initial phase (6 min) and over the domain of the experiment (30 min) is presented in Fig 7. The ascending order of different nanofluids in terms of their overall experimental photothermal performance is  $\text{Al}_2\text{O}_3\text{-}\gamma$ , Si, Cu, Zn, Fe and Ag based on 6 min and 30 min data shown in Fig. 7 (a) and Fig. 7 (b) respectively. It can be concluded from Fig. 7 (b) that the efficiency of sensible heating for all the nanofluids is almost the same with little variation over 30 min duration of exposure to solar flux and the major difference in between lies on the evaporation effect. As revealed from Jin et al. (2016a, 2016b), there was large temperature difference inside nanofluids under solar radiation, and the major effect for nanofluids lies on the trapping of solar energy, especially at the surface layer. Under strong solar radiation (i.e. a few hundred of Suns), the surface layer could become superheated and vigorous boiling could occur, albeit the bulk fluid is still under subcooled condition. The current study revealed a similar trend. Although the temperature was not high enough to cause vigorous boiling, the major difference among different nanofluids lies on the surface trapping and evaporation effect. The difference in heating the bulk fluids, as shown by the sensible heating efficiency, is small among different nanofluids. Most of the extra heat converted by nanoparticles is used to evaporate the fluid, which mainly occurs at the surface. The higher the surface temperature, the higher the

evaporation rate. Consequently, different nanofluids should be identified for different applications. Taking desalination as an example, highly non-uniform temperature is preferred (i.e. focusing heat on the surface) by using suitable nanoparticles, so most of the converted heat can be used to evaporate instead of heating the bulk fluid.

The capability of the nanoparticles for this localized heating can also be determined by their specific absorption rate (SAR), which is the ability of the nanoparticle unit mass to absorb energy in given time. SAR value for silver nanoparticles is the highest amongst all compared nanomaterials in this study (Fig. 9), followed by Fe and Zn nanofluids. The phenomenon of localized heating is the highest in case of silver nanofluid due its strong plasmonic nature.

## **5. Conclusion**

Light to heat conversion capabilities of various nanofluids have been investigated experimentally under the focused light of a solar simulator. It was found quantitatively that the addition of small fraction of nanoparticle in the base fluid can significantly enhance its photothermal conversion performance. Comparing with the base fluid, the increasing order of nanofluids in this investigation was  $\text{Al}_2\text{O}_3\text{-}\gamma$ , Si, Cu, Zn, Fe and Ag , and the major difference lied on the evaporation efficiency. The enhanced performance of nanofluid was described in terms of sensible and latent heat contribution to the photothermal behavior. Silver nanofluid achieved the maximum enhancement of 99.7% in photothermal conversion efficiency compared to the base fluid.

## **Acknowledgement**

To be inserted. include the British council support

## References

1. Gupta, H.K., G.D. Agrawal, and J. Mathur, *An experimental investigation of a low temperature Al<sub>2</sub>O<sub>3</sub>-H<sub>2</sub>O nanofluid based direct absorption solar collector*. Solar Energy, 2015. **118**: p. 390-396.
2. Said, Z., et al., *Performance enhancement of a Flat Plate Solar collector using Titanium dioxide nanofluid and Polyethylene Glycol dispersant*. Journal of Cleaner Production, 2015. **92**: p. 343-353.
3. Sokhansefat, T., A.B. Kasaeian, and F. Kowsary, *Heat transfer enhancement in parabolic trough collector tube using Al<sub>2</sub>O<sub>3</sub>/synthetic oil nanofluid*. Renewable and Sustainable Energy Reviews, 2014. **33**: p. 636-644.
4. Salavati Meibodi, S., et al., *Experimental investigation on the thermal efficiency and performance characteristics of a flat plate solar collector using SiO<sub>2</sub>/EG-water nanofluids*. International Communications in Heat and Mass Transfer, 2015. **65**: p. 71-75.
5. Liu, J., et al., *A combined numerical and experimental study on graphene/ionic liquid nanofluid based direct absorption solar collector*. Solar Energy Materials and Solar Cells, 2015. **136**: p. 177-186.
6. Minardi, J.E. and H.N. Chuang, *Performance of a "black" liquid flat-plate solar collector*. Solar Energy, 1975. **17**(3): p. 179-183.
7. Chen, M., et al., *An experimental investigation on sunlight absorption characteristics of silver nanofluids*. Solar Energy, 2015. **115**: p. 85-94.
8. Luo, Z., et al., *Performance improvement of a nanofluid solar collector based on direct absorption collection (DAC) concepts*. International Journal of Heat and Mass Transfer, 2014. **75**: p. 262-271.
9. Mahian, O., et al., *A review of the applications of nanofluids in solar energy*. International Journal of Heat and Mass Transfer, 2013. **57**(2): p. 582-594.
10. Bandarra Filho, E.P., et al., *Experimental investigation of a silver nanoparticle-based direct absorption solar thermal system*. Energy Conversion and Management, 2014. **84**: p. 261-267.
11. Eustis, S. and M.A. El-Sayed, *Why gold nanoparticles are more precious than pretty gold: Noble metal surface plasmon resonance and its enhancement of the radiative and nonradiative properties of nanocrystals of different shapes*. Chemical Society Reviews, 2006. **35**(3): p. 209-217.
12. Pérez-Juste, J., et al., *Gold nanorods: Synthesis, characterization and applications*. Coordination Chemistry Reviews, 2005. **249**(17-18): p. 1870-1901.
13. Zhang, H., et al., *Photothermal conversion characteristics of gold nanoparticle dispersions*. Solar Energy, 2014. **100**: p. 141-147.
14. Rahman, M.M., et al., *Effect of solid volume fraction and tilt angle in a quarter circular solar thermal collectors filled with CNT-water nanofluid*. International Communications in Heat and Mass Transfer, 2014. **57**: p. 79-90.
15. Said, Z., et al., *Analyses of exergy efficiency and pumping power for a conventional flat plate solar collector using SWCNTs based nanofluid*. Energy and Buildings, 2014. **78**: p. 1-9.
16. Yousefi, T., et al., *An experimental investigation on the effect of pH variation of MWCNT-H<sub>2</sub>O nanofluid on the efficiency of a flat-plate solar collector*. Solar Energy, 2012. **86**(2): p. 771-779.
17. He, Q., et al., *Experimental investigation on photothermal properties of nanofluids for direct absorption solar thermal energy systems*. Energy Conversion and Management, 2013. **73**: p. 150-157.
18. Gupta, H.K., G.D. Agrawal, and J. Mathur, *Investigations for effect of Al<sub>2</sub>O<sub>3</sub>-H<sub>2</sub>O nanofluid flow rate on the efficiency of direct absorption solar collector*. Case Studies in Thermal Engineering, 2015. **5**: p. 70-78.

19. Mahian, O., et al., *Entropy generation during Al<sub>2</sub>O<sub>3</sub>/water nanofluid flow in a solar collector: Effects of tube roughness, nanoparticle size, and different thermophysical models*. International Journal of Heat and Mass Transfer, 2014. **78**: p. 64-75.
20. Said, Z., et al., *Experimental investigation of the thermophysical properties of AL<sub>2</sub>O<sub>3</sub>-nanofluid and its effect on a flat plate solar collector*. International Communications in Heat and Mass Transfer, 2013. **48**: p. 99-107.
21. Yousefi, T., et al., *An experimental investigation on the effect of Al<sub>2</sub>O<sub>3</sub>-H<sub>2</sub>O nanofluid on the efficiency of flat-plate solar collectors*. Renewable Energy, 2012. **39**(1): p. 293-298.
22. Otanicar, T.P., et al., *Nanofluid-based direct absorption solar collector*. Journal of Renewable and Sustainable Energy, 2010. **2**(3): p. 033102.
23. Hewakuruppu, Y.L., et al., *Limits of selectivity of direct volumetric solar absorption*. Solar Energy, 2015. **114**: p. 206-216.
24. Lee, B.J., et al., *Radiative Heat Transfer Analysis in Plasmonic Nanofluids for Direct Solar Thermal Absorption*. Journal of Solar Energy Engineering, 2012. **134**(2): p. 021009.
25. Lee, S.-H., et al., *Extinction coefficient of water-based multi-walled carbon nanotube nanofluids for application in direct-absorption solar collectors*. Micro & Nano Letters, 2014. **9**(10): p. 635-638.
26. Saidur, R., et al., *Evaluation of the effect of nanofluid-based absorbers on direct solar collector*. International Journal of Heat and Mass Transfer, 2012. **55**(21-22): p. 5899-5907.
27. Tyagi, H., P. Phelan, and R. Prasher, *Predicted Efficiency of a Low-Temperature Nanofluid-Based Direct Absorption Solar Collector*. Journal of Solar Energy Engineering, 2009. **131**(4): p. 041004.
28. Zhang, L., et al., *Radiative properties of ionic liquid-based nanofluids for medium-to-high-temperature direct absorption solar collectors*. Solar Energy Materials and Solar Cells, 2014. **130**: p. 521-528.
29. Zhang, H., et al., *Dependence of Photothermal Conversion Characteristics on Different Nanoparticle Dispersions*. Journal of Nanoscience and Nanotechnology, 2015. **15**(4): p. 3055-3060.
30. Wen, D., *Intracellular hyperthermia: Nanobubbles and their biomedical applications*. International Journal of Hyperthermia, 2009. **25**(7): p. 533-541.
31. Otanicar, T.P., P.E. Phelan, and J.S. Golden, *Optical properties of liquids for direct absorption solar thermal energy systems*. Solar Energy, 2009. **83**(7): p. 969-977.
32. Otanicar, T.P., et al., *Spatially Varying Extinction Coefficient for Direct Absorption Solar Thermal Collector Optimization*. Journal of Solar Energy Engineering, 2011. **133**(2): p. 024501.
33. Mercatelli, L., et al., *Absorption and scattering properties of carbon nanohorn-based nanofluids for direct sunlight absorbers*. Nanoscale Research Letters, 2011. **6**(1): p. 1-9.

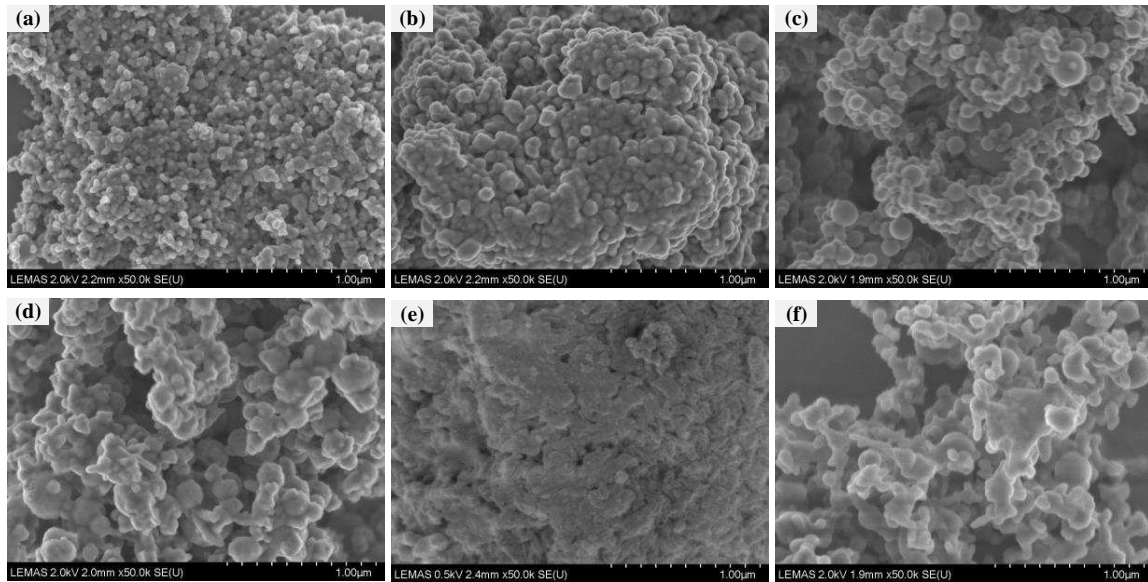
include all relevant papers in our group (check my publication list)m including

Jin et al. Nano Energy

Jin et al. Solar Energy .....

## List of Figures and tables

**(I)**



**(II)**

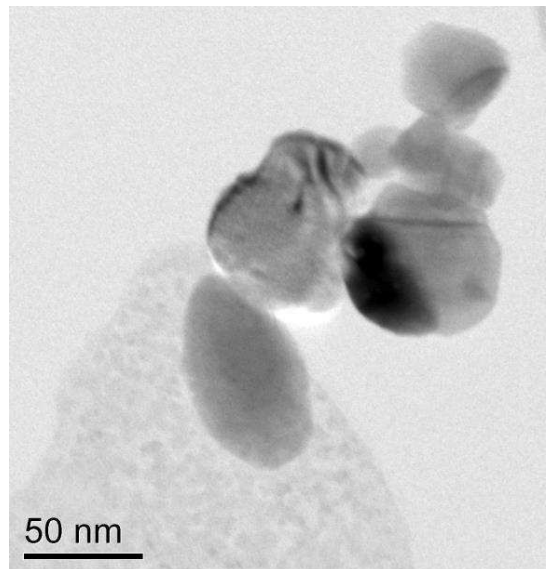


Fig. 1 Morphological appearance of nanopowders **(I)** SEM images of nanopowders of (a) Copper, (b) Silver, (c) Iron, (d) Zinc, (e) Aluminum oxide- $\gamma$  and (f) Silicon and **(II)** TEM micrograph of silver nanoparticles dispersed in deionized water.

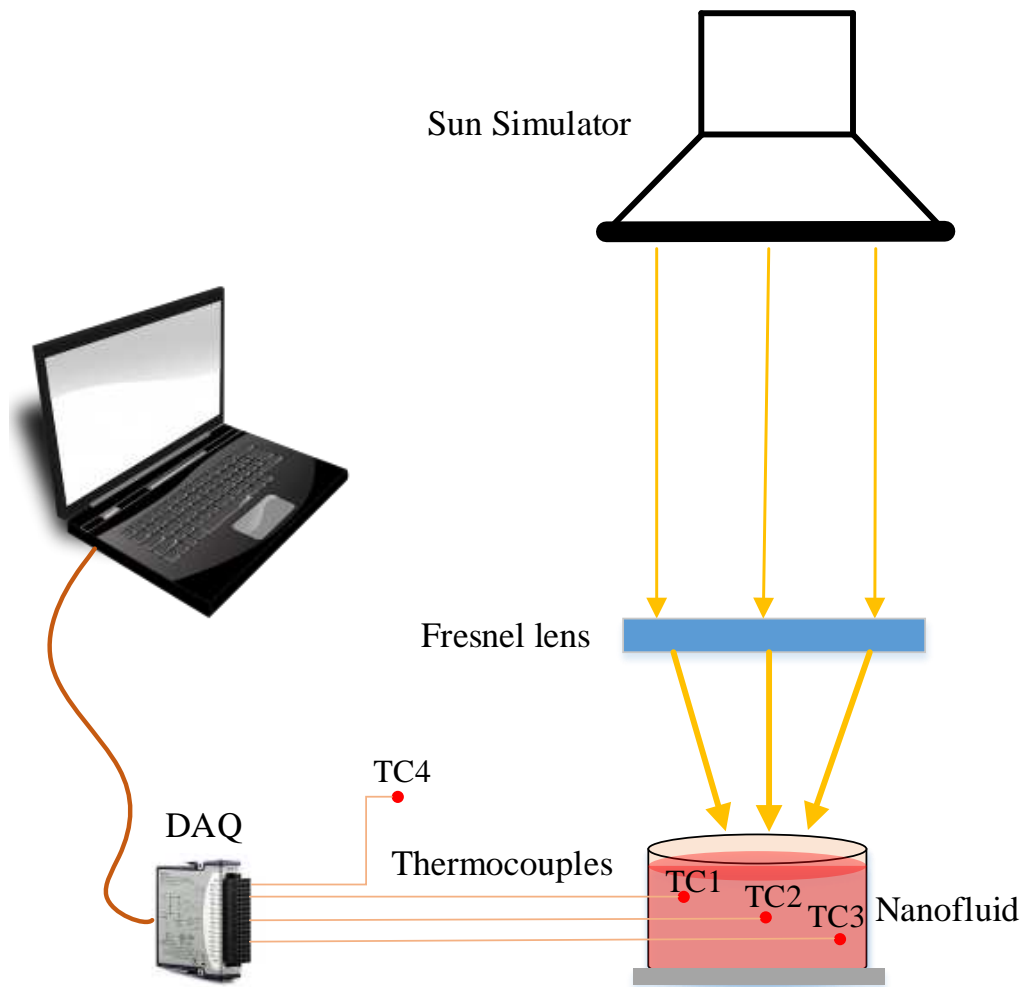


Fig. 2 Schematic view of the experimental setup showing the position of thermocouples and arrangement of Fresnel lens under a solar simulator

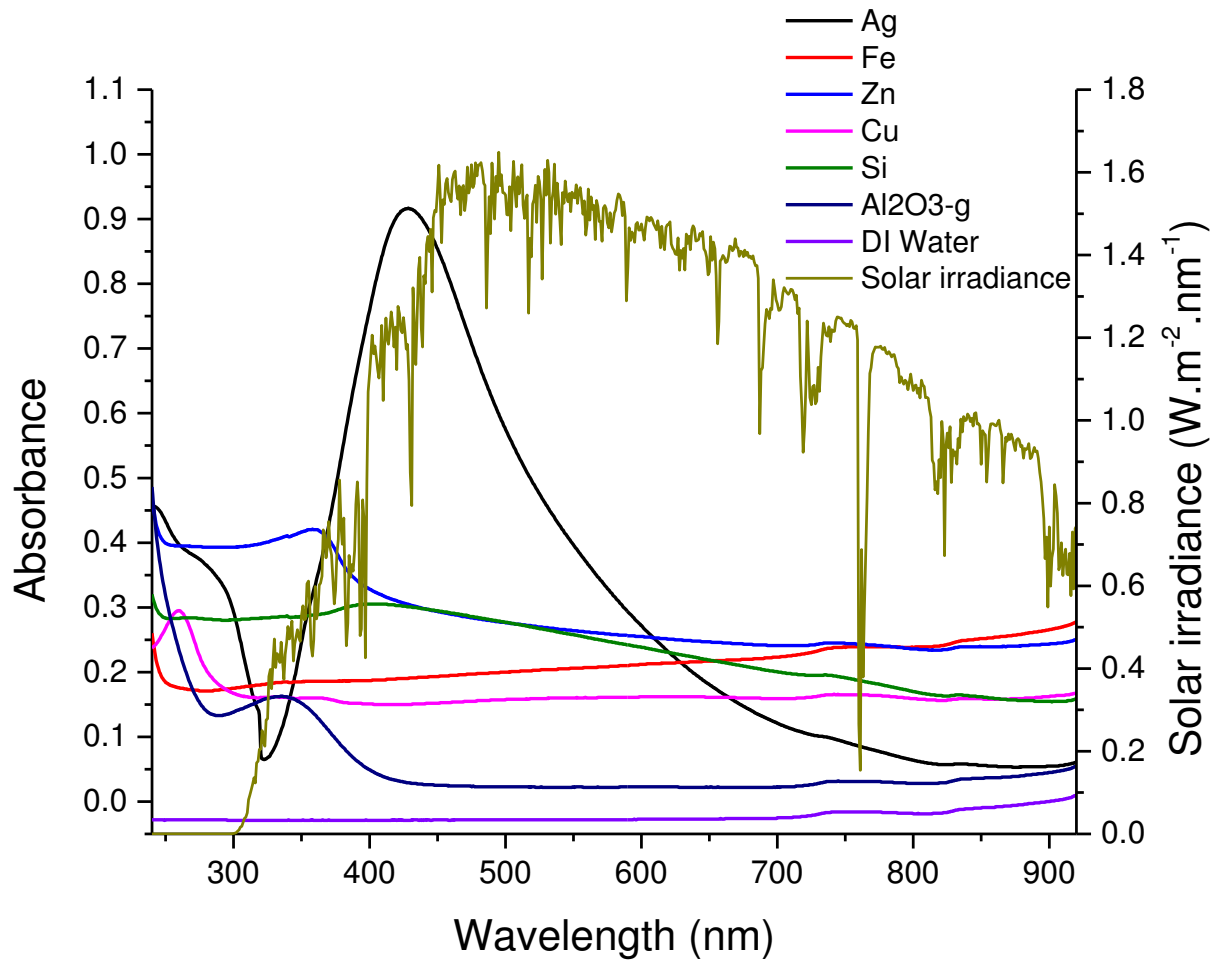


Fig. 3 Optical absorbance spectra of DI water based nanofluids (0.01 wt%) in the UV to Visible spectrum.

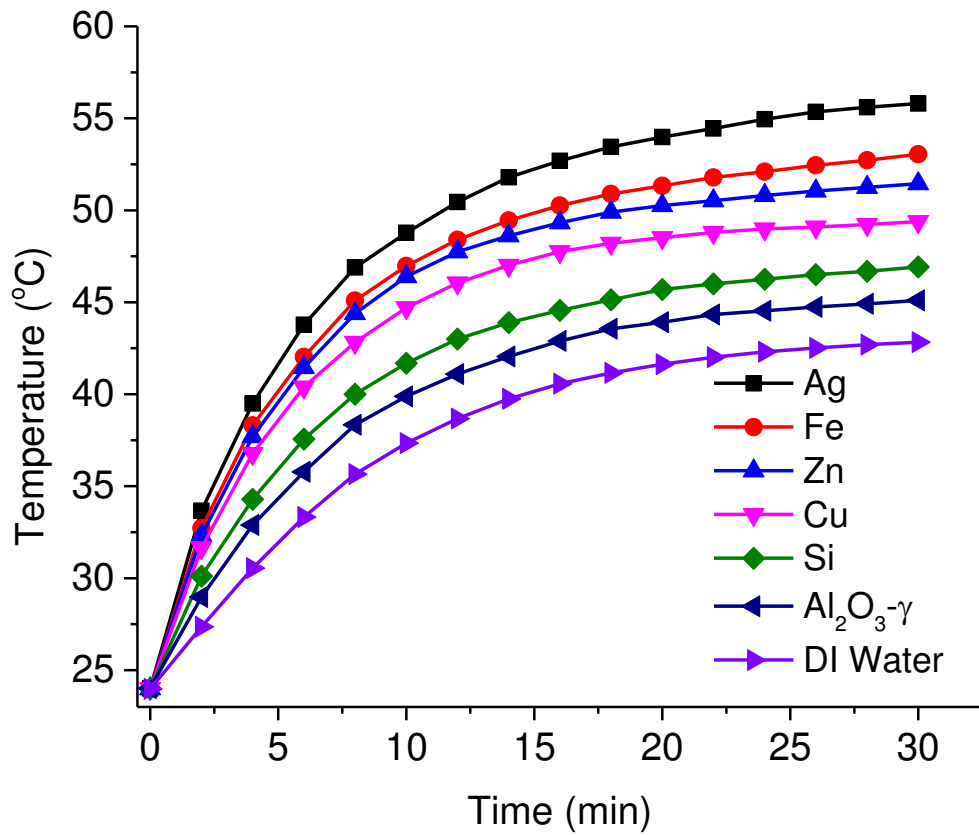


Fig. 4 Average transient temperature profiles of various nanofluid samples with 0.01% weight concentration under a solar intensity of 12 Suns and comparison to that of deionized water.

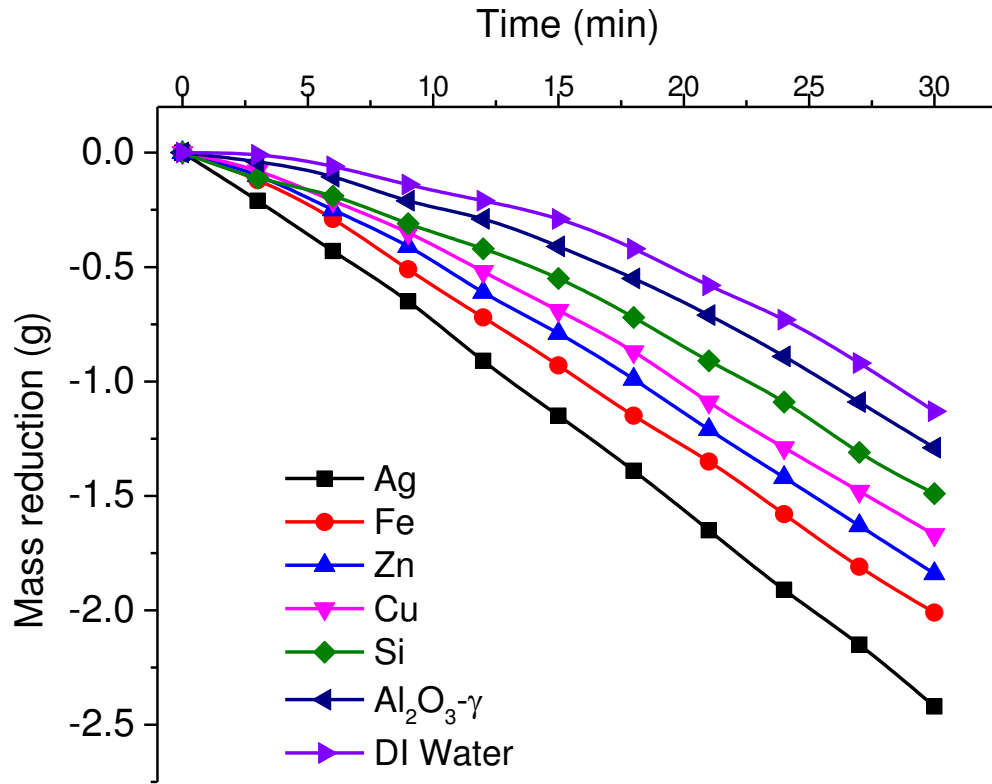


Fig. 5 Mass loss as a function of time for various nanofluids under a solar intensity of 12 Suns over a period of 30 min.

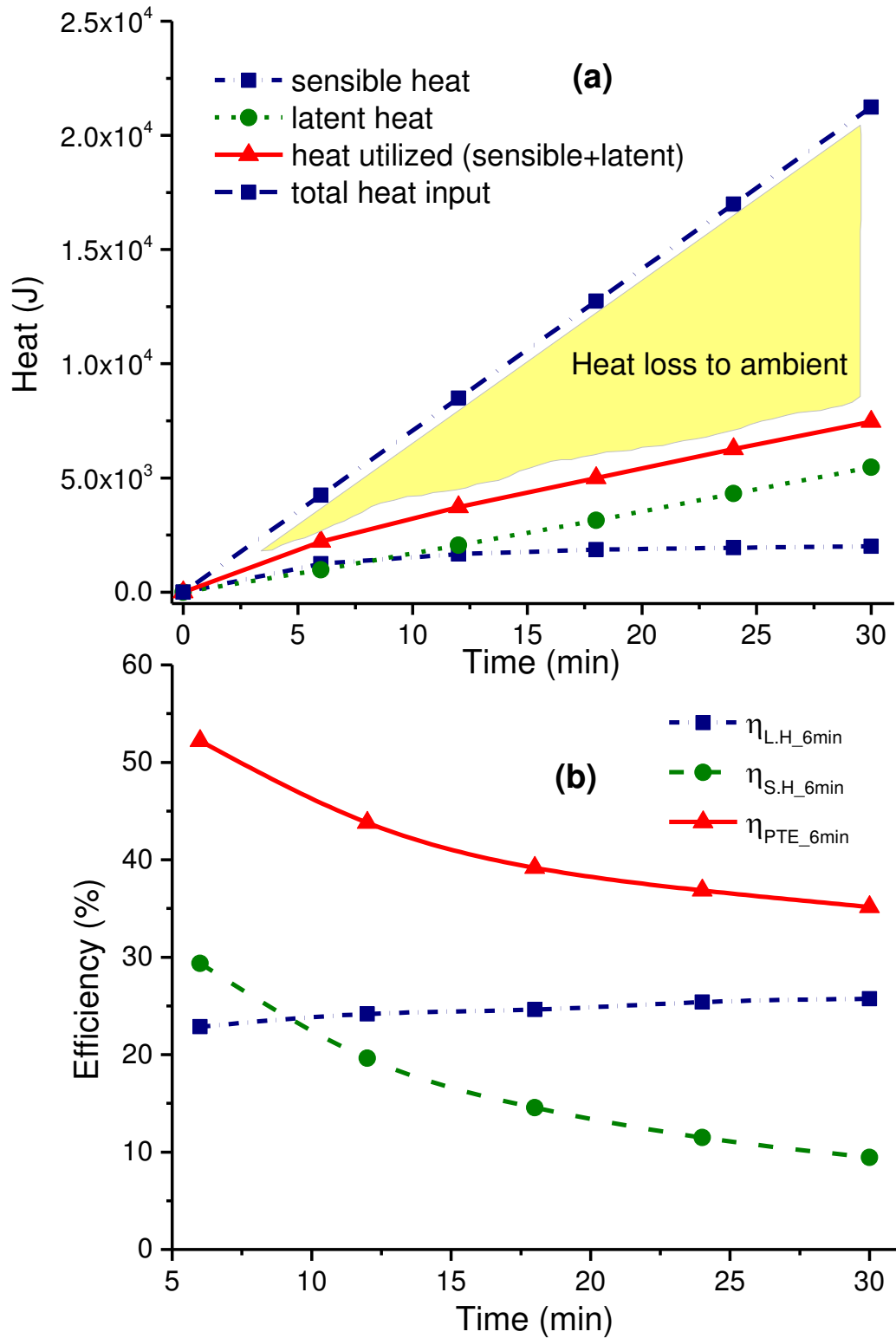


Fig. 6 Photothermal performance of silver nanofluid over a period of 30 minutes , (a) contribution of sensible heating and latent heating, and (b) variation of sensible heating and

latent heating efficiencies ( $\eta_{S.H}$  and  $\eta_{L.H}$  respectively) and overall photothermal efficiency ( $\eta_{PTE}$ ).

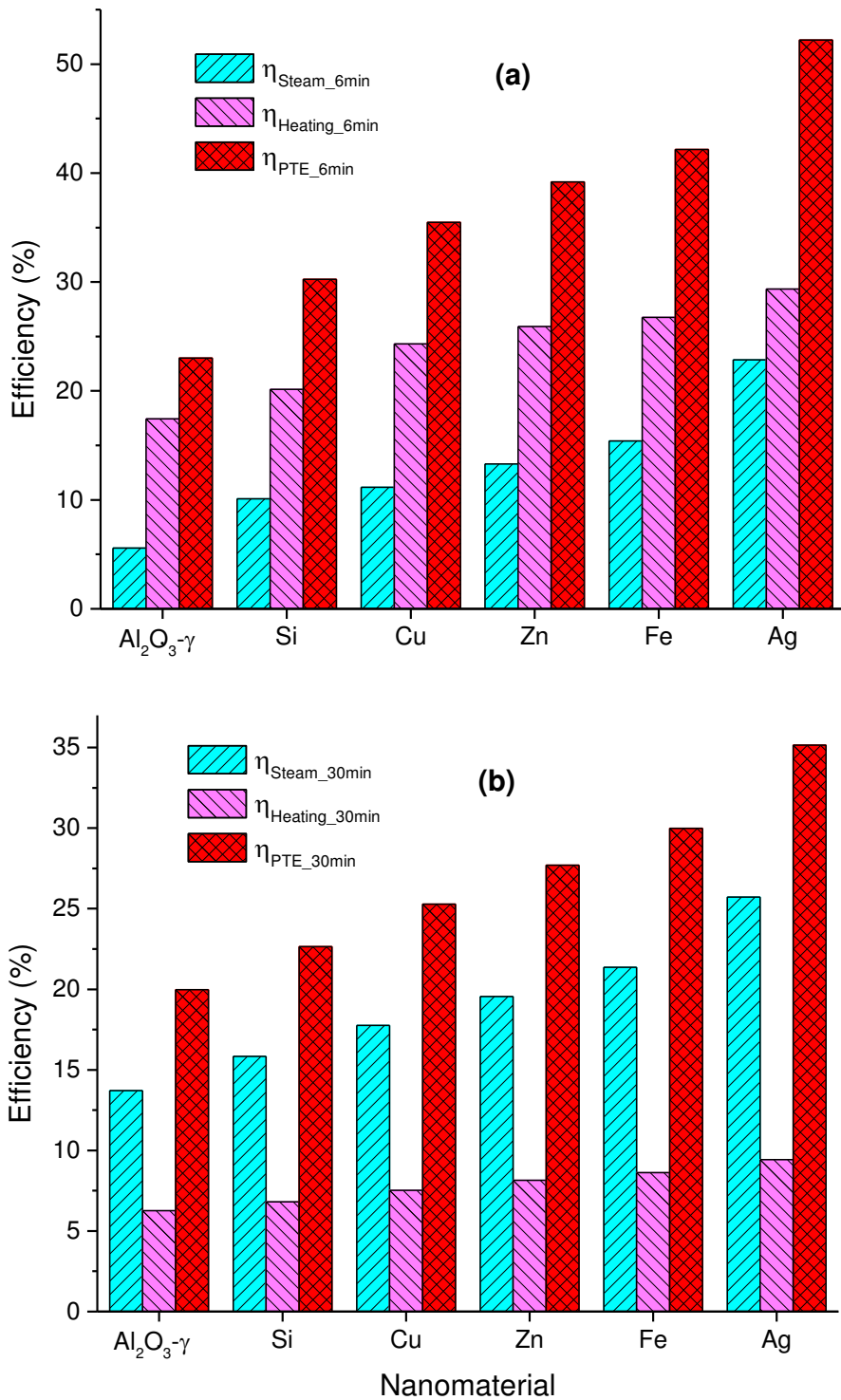


Fig. 7 Distribution of Photothermal conversion efficiency of various nanofluids into sensible heat efficiency and evaporation efficiency based on the data of (a) first 6 min and (b) 30 min

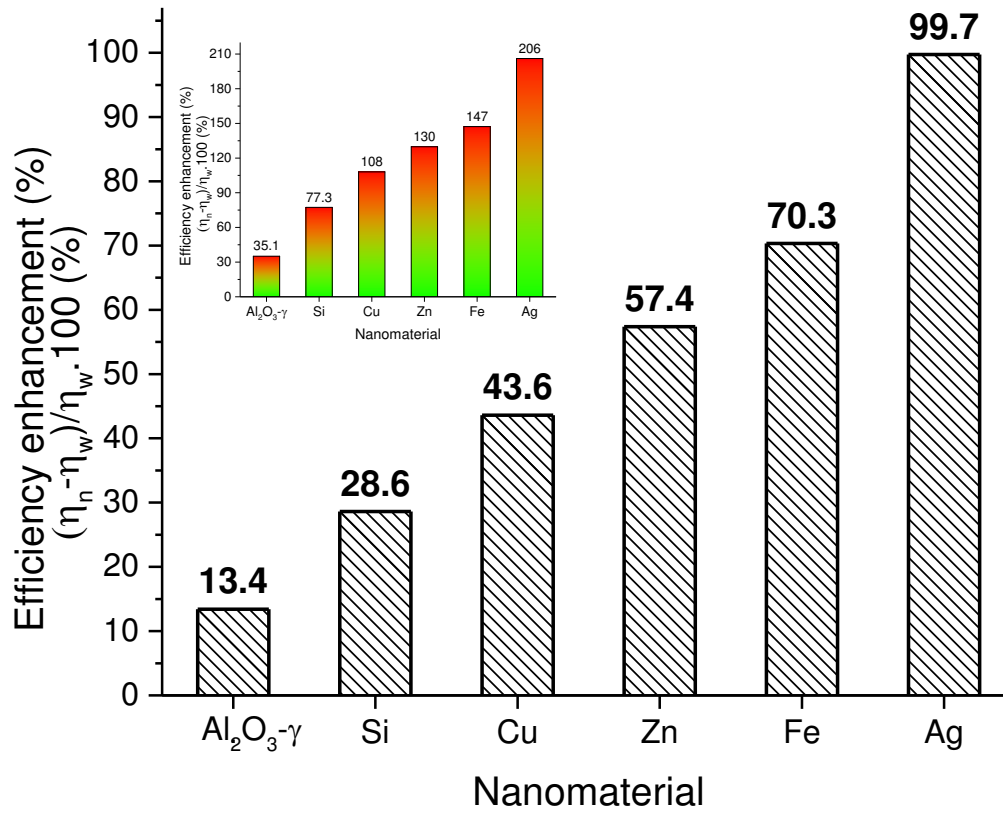


Fig. 8 Overall enhancement in photothermal conversion efficiency over the base fluid for full experimental duration (i.e. 30 mins). The enhancement for first 6 min of the experiment is even higher, which is also shown as the insert .

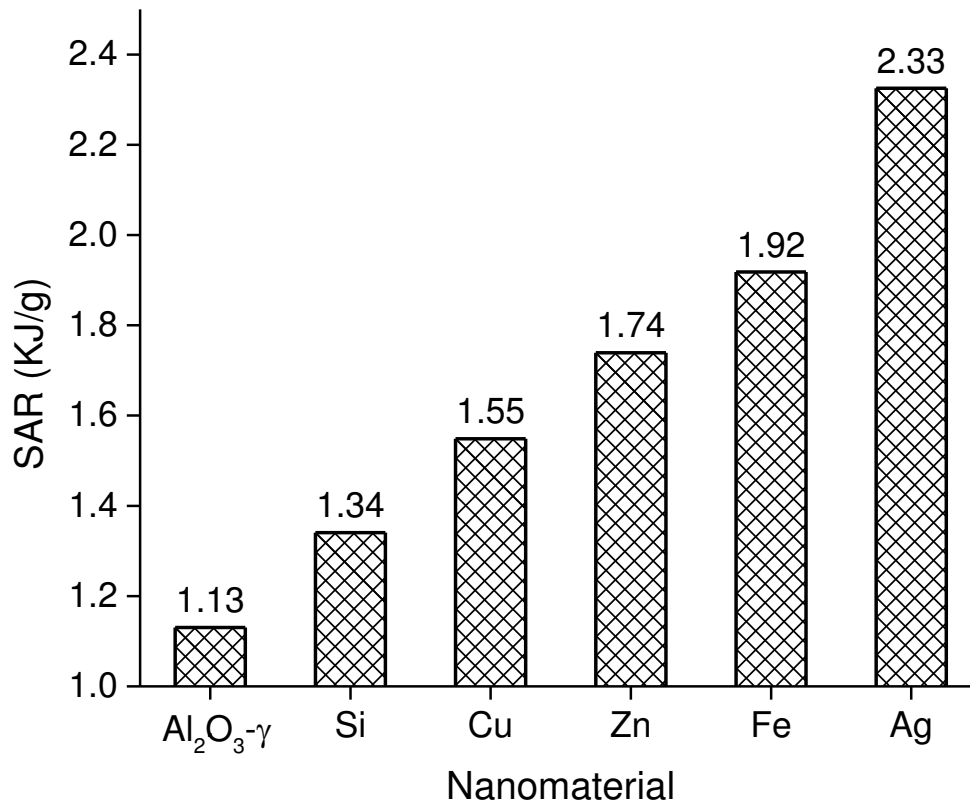


Fig. 9 Specific absorption rate of nanofluids based on data shown in Fig. 4

Table 1. Size range of various nanofluids

<b>Nanomaterial</b>	<b>size range</b>	<b>Supplier</b>
Cu	35-45 nm	Sigma Aldrich
Ag	50-60 nm	Sigma Aldrich
Zn	40-60 nm	Sigma Aldrich
Si	30-50 nm	Nanostructured & amorphous material Inc.
Fe	50-80 nm	Nanostructured & amorphous material Inc.
Al <sub>2</sub> O <sub>3</sub> -γ	40-80 nm	Nanostructured & amorphous material Inc.